Improvement of Reading Performance of Frequency-Domain Chipless RFID Transponders

Jaroslav HAVLICEK, Milan SVANDA, Jan MACHAC, Milan POLIVKA

Dept. of Electromagnetic Field, Czech Technical University in Prague, Technicka 2, 166 27, Prague, Czech Republic

{havlij18, svandmil, machac, polivka}@fel.cvut.cz

Manuscript received May 09, 2016

Abstract. *This review paper presents the summary of our investigations in several topics of frequency-domain chipless RFID transponders. The performance comparison of various types of scatterers used in the literature and recently proposed by the authors is presented. The issue of proper location of adjacent resonant elements in the scatterer array to reduce the mutual coupling and consequently ensure the robust RCS response for reliable reading of coded information is addressed. A major improvement in RCS response of transponders is proposed, using slot-in-plate type transponders. Advantages and drawbacks of the proposed solutions are discussed and several open challenges in the field are emphasized.*

Keywords

Chipless RFID, mutual coupling, monostatic RCS measurement, scatterer

1. Introduction

The radiofrequency identification (RFID) is a widespread technology, which is applied mainly in industry (production process monitoring), logistics (acceleration of storing procedures), commerce (antitheft feature), health care (elimination of patient confusions) and inventorying (e.g. books in libraries). RFID is expected to have an important role in the internet of things concept [1]. There is a perfect opportunity for further spreading in commerce, provided that the RFID transponders (tags) are suitable for optical barcode replacement [2]. The advantage of the tag consists in the possibility to be read without necessity of clear line of sight. Indeed, its low price is essential for reaching this goal. Unfortunately conventional tags consisting of chips are about hundred times more expensive than the ones equipped with barcodes [3]. Yet a chipless RFID [4], which provides different methods of storing identification information without chip, represents a promising way how the tag cost can be reduced. The most promising methods are those, whose layouts allow the tag production by means of printing, using a suitable conductive ink, for the price of printable tags can be potentially comparable to the one of optical barcodes. These methods can be separated into two main groups (Fig. 1.), i.e. the tags based on time domain detection on one hand and tags based on frequency domain detection on the other.

The operational principle of tags with time domain detection is identical to the conventional chip tag principle. The identification information is received as a set of pulses with different time spacing between them. Representatives of such kind of tag are SAW (Surface Acoustic Wave) [5], TFTC (Thin Film Transistor Circuit) technology [6] and tags with delay line [7], [8]. The SAW tag is already commercially available, but its price is not comparable with an optical barcode although it is cheaper than a conventional chip tag. The TFTC technology's potential advantages consist in a rewritable memory and compatibility with conventional RFID readers, which are already in usage. Tags with delay line suffer from an insufficient bit capacity.

Chipless tags based on the frequency domain detection, involving planar resonators in most cases, represent promising examples of this technology. The presence or absence of each resonator's peak in tag's spectral signature represents one or zero bit information, respectively. The low bit capacity of tags represents the key issue to be resolved. Representatives of this group are approaches using nanometric materials [9], electric tattoo ink [10], space fitting curves [11] and various types of LC resonators [12–16]. The idea of ink with different magnetic properties caused by adding nanometric particles for shaping spectral signature was proposed in 2004 by CrossID company. The electronic tattoo ink (applied mainly for animal tagging) was about to be developed in 2009 by Somark company. The development of both of these approaches seems to be suspended, since CrossID ceased to exist and Somark specializes merely in the field of marking laboratory mice (only visual tattoo) [17]. Planar space fitting curves such as Peano or Hilbert curve can be also used for chipless RFID. Their advantage is embodied in a high level of electric length reduction, which is beneficial for miniaturization. The disadvantage, however, lies in the necessity of complicated tag layout changes for coding different bit numbers. The latter subgroup might be generally labeled as 'LC resonators' and is considered the most promising, given the

DOI: 10.13164/re.2016.0219

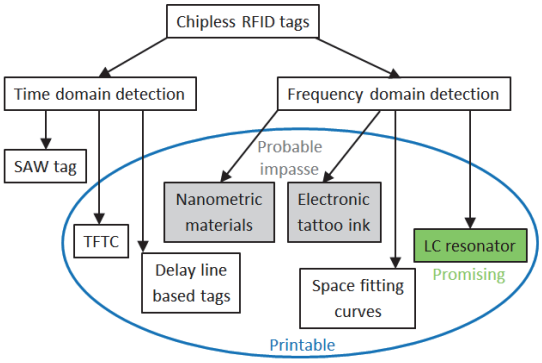

Fig. 1. Chipless RFID technology overview.

enormous variety of possible chipless RFID solutions. These tags can be also used as chipless sensors [18–20].

In Sec. 2, the performance comparison in terms of the electrical size, radar cross section (RCS) magnitude, and bandwidth of various types of planar scatterers used as chipless RFID tag building elements is presented. Section 3 addresses a crucial aspect of small scatterer arrays of U-folded dipoles, i.e. – improvement in robustness and readability of their RCS response by reducing the inter-element mutual coupling. This can be done by rearrangements of adjacent resonant elements into distant positions or by inclination of their arms. Both methods are compared, and their influence on amplitude and frequency stability of RCS response is discussed. The increase in overall RCS response using slot-in-plate type chipless RFID tags is presented and discussed in Sec. 4. The employed monostatic RCS measurement method is briefly described in Sec. 5. The final section summarizes the lessons learned, suggests few design hints, and emphasizes several open challenges in the field of frequency-domain chipless RFID.

2. Scatterers Based on LC Resonators

Many different types of planar resonators serving as basic building units of chipless RFID tag with frequency domain detection can be found in the open literature. We can specify three principal quantities, which must be investigated for each resonator. The radar cross-section (RCS) that determines the reading range of the tag is the first of them. It can be seen that a higher RCS results in a longer reading range. The bandwidth (BW) of resonance peak depending on the quality factor Q of the resonance represents the second quantity. Its evaluation can be performed from frequency characteristics of the resonator as a frequency range of three-decibel resonance peak drop. This characteristic is very important from the spectral bit capacity point of view. The product ka is the last one from the above-mentioned quantities. The variable k is the wave number, while the variable a stands for the radius of circle that circumscribes the resonator. This product represents the rate of electric reduction of the resonator. Resonators with ka below one are more suitable candidates, because small size is essential for application in chipless RFID.

2.1 Topology of Investigated Scatterers

This section deals with the performance comparison of planar resonators. It is based on the aforementioned three essential characteristics; see Fig. 2 and 3. Examples of this category are specified in the following table and text.

Scatterer	Size
Dipole	length 37 mm, width 1 mm
Circular ring	diameter 10 mm, line width 1 mm, gap width 2.3 mm
Rectangular ring	side 10 mm, line width 1 mm, split length 2.5 mm
Meander dipole	total length 56 mm, meander length 6 mm, line width 1 mm, distance between meanders 1 mm
Thick U dipole [13]	arm length 20.5 mm, line width 1 mm, distance between arms 0.5 mm
Thin U dipole [21]	arm length 20.5 mm, line width 0.25 mm, distance between arms 2 mm
Skew arms U dipole [21]	arm length 20.5 mm, line width 0.25 mm, distance between skew arms at their open ends 0.5 mm
Meander U dipole [22]	arm length 20.5 mm, line width 0.25 mm, meander length 5 mm, distance between meander arms 0.2 mm, distance between dipole arms 2 mm

Tab. 1. Topology and size of investigated scatterers.

Another group of scatterers is represented by several capacitively loaded dipoles and one inductively loaded dipole (ILD). All these scatterers occupy a rectangle area ranging from 20.5 mm to 2.5 mm. ILD consists of 18 skew parts. The spacing between them and the arms is 0.23 mm in length, line width equals 0.25 mm and length of the straight part in the middle of the scatterer is equal to 2 mm. The basic capacitively loaded dipole (CLD 1) consists only of a dipole part and four loading arms of 9.25 mm in length each. The spacing between the dipole part and the arms equals 0.88 mm and the width of all lines accounts for 0.25 mm. The version labeled as CLD 2 is based on CLD 1, yet four inner arms were added (length of 8.75 mm, spacing between dipole part and inner arms is 0.38 mm, spacing between outer and inner arms equals 0.26 mm).

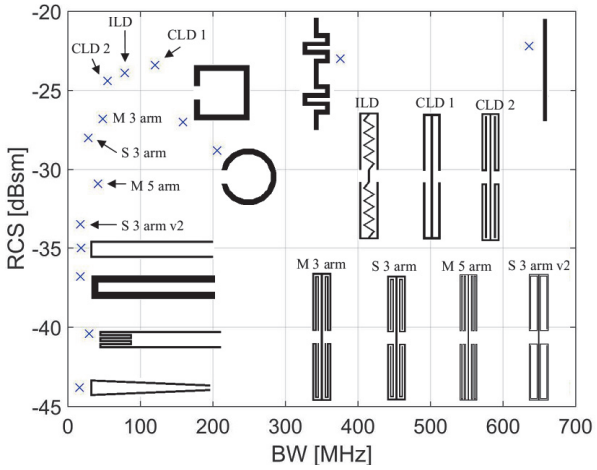

Fig. 2. Comparison of scatterers according to RCS and resonance bandwidth.

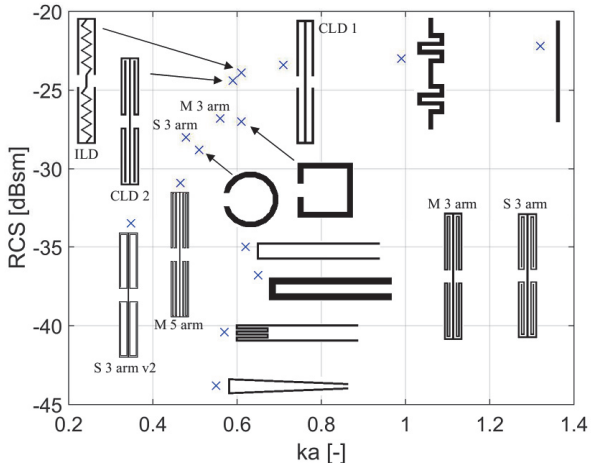

Fig. 3. Comparison of scatterers according to RCS and *ka* product.

The capacitively loaded dipoles can be divided into two groups. The difference lies in the mutual linking of ending arms, which can be either mender or spiral-shaped. We proposed three-arm versions labeled as 'M 3 arm' and 'S 3 arm'. The latter represent an extension of CLD 2 (arms width as well as spacing between them was reduced to 0.18 mm). Thin versions (M 5 arm and S 3 arm v2) have five and three arms respectively and their line width as well as spacing between arms equals 0.1 mm. The layouts of all proposed scatterers are shown in Figs. 2 and 3. All scatterers were designed on Rogers RO4003 woven-glass laminate ($\varepsilon_r = 3.38$, $\tan\delta = 0.002$, 0.2 mm in thickness).

2.2 Performance Comparison of Scatterers

In conformity with the theory of electrically small antennas, it can be stated that the resonance structures with small *ka* show high levels of quality factor *Q*. This phenomenon results in a low frequency bandwidth on one hand (this is beneficial for high spectral bit capacity), yet in low RCS on the other, which is inappropriate for reading range. Therefore the chipless RFID tag design consists always in searching for the balanced trade-off between the spectral bit capacity and the reading. The simulated performance comparison of scatterers properties in method of moment software Zeland IE3D are shown in Tab. 2. Figures 2 and 3 confirm this statement.

Scatterer	*ka* [-]	f_r [GHz]	RCS_{max} [dBsm]	BW [MHz]
Dipole	1.32	3.400	–22.2	636.0
Circular ring	0.51	4.893	–28.8	205.7
Rectangular ring	0.61	4.085	–27.0	158.8
Meander dipole	0.99	3.555	–23.0	375.6
Thick U dipole	0.65	3.012	–36.8	17.2
Thin U dipole	0.62	2.855	–35.0	18.2
Skew arms U dip.	0.55	2.565	–43.8	16.0
Meander U dipole	0.57	2.623	–40.4	29.2
CLD 1	0.71	3.263	–23.4	120.2
CLD 2	0.59	2.723	–24.4	54.7
M 3 arm	0.56	2.570	–26.8	48.1
ILD	0.61	2.830	–23.9	78.3
S 3 arm	0.48	2.212	–28.0	28.1
M 5 arm (thin)	0.47	2.152	–30.9	41.5
S 3 arm v2 (thin)	0.35	1.609	–33.5	17.2

Tab. 2. Comparison of scatterer properties operating at their resonant frequency.

U dipoles achieved the lowest frequency bandwidth, above all the skew dipole with bandwidth 16 MHz. However, their RCS response is below or equal to –35 dBsm, which leads to a shorter reading range. Their coefficients *ka* attain average levels.

The capacitively loaded dipoles show, in general, better RCS (up to –23.4 dBsm), however most of them are insufficient from the frequency bandwidth point of view. When comparing CLD 1, CLD 2 and M/S 3 arm scatterers, it is noticeable that adding more arms to the scatterer endings results in the higher *ka* and lower BW, yet at the expense of RCS magnitude.

The comparison of meander/spiral approaches shows that when taking into account the employment of chipless RFID, the spiral scatterer has more suitable properties. This phenomenon is attributable to the orientation of coincident currents in neighboring arms of the spiral, compared to the opposite currents in meander arms [23]. Thin variants of meander/spiral scatterers were designed in more than two versions proposed above, however their RCS was too low or the frequency bandwidth was too high, hence they turned out to be unsuitable for multi-bits chipless structures.

2.3 Tag Arrangements

The S3 arm v2 dipole scatterer was chosen for the design of a 5-bit tag due to its very low bandwidth, which represents an important advantage, although the RCS of this structure is average at the level –33 dBsm. The mutual coupling between particular scatterers represents a fundamental problem for tag design and reliable function. There are two arrangements of 5-bits tag proposed in this section. For basic side-by-side arrangement, where the mutual coupling is reduced only by $l_h = 4.5$ mm spacing between the neighboring scatterers, see Fig. 4(a). The size of this arrangement is 34.5×24.5 mm^2. The second arrangement is focused on more efficient reduction of mutual coupling using parallel-in-echelon of each scatterer by $l_v = 21.5$ mm; see Fig. 4(b). The size of this is 20.5×109 mm. The frequency spacing between resonances equals 100 MHz in both cases; see Fig. 5.

As it can be seen in Fig. 5, the mutual coupling in side-by-side arrangement leads to differences in amplitudes of each resonance and also (much less significant) shifts in their frequency. They are more significant in horizontal tag arrangement. The saw-toothed shape of resonances represents another consequence of the strong scatterers mutual coupling in this arrangement.

The measured results are plotted in Fig. 6. The RCS responses of both variants of 5-bit chipless RFID tags correspond to the simulated properties depicted in Fig. 5.

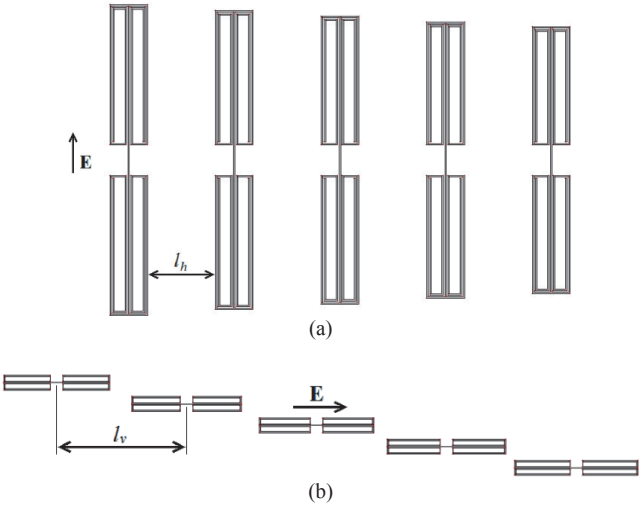

Fig. 4. Designed 5-bit tags with side-by-side arrangement (a) and parallel-in-echelon arrangement (b).

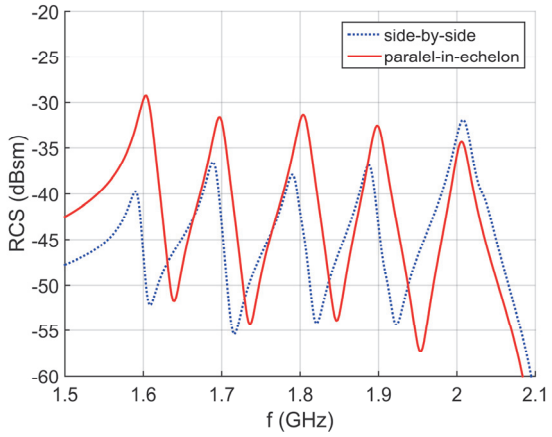

Fig. 5. Simulated performance of 5-bit tags in both arrangements.

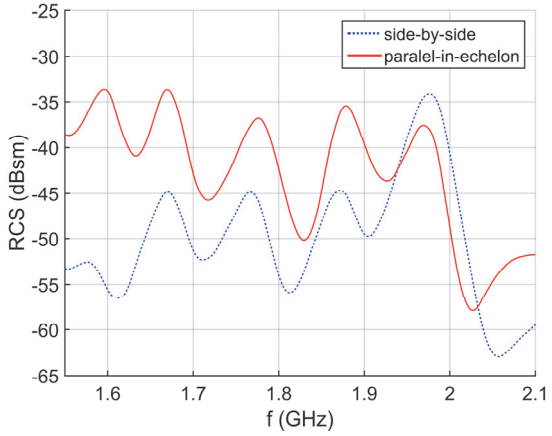

Fig. 6. Measured performance of 5-bit tags in both arrangements.

The amplitude differences in resonances of the side-by-side arrangement are more significant in case of the measurement results. The frequency shift (of approx. 20 MHz) and amplitude difference (roughly 5 dB) between the simulated and measured data can be observed. This phenomenon is namely caused by the limitation of simulation in the case that the infinite substrate in method of moments is used, while the real footprint size of the supporting dielectric plate is 28 × 44 mm^2 (for side-by-side arrangement) and 24 × 112 mm^2 (for parallel-in-echelon arrangement).

3. Improvement in Robustness and Readability by Reduction in Inter-Element Mutual Coupling

The mutual coupling between scatterers is a major obstacle to achieve a high bit capacity tag, see Sec. 2.3. Two methods for reduction of this negative effect are presented below. The first one is based on the scatterer topology modification. In fact, there is a trade-off between the reduction in mutual coupling and attainment of maximum RCS response. The other method applies the rearrangement, which reduces the mutual coupling by maximizing the distance between scatterers that are neighboring in terms of frequency. The mutual coupling reduction effect of both methods is demonstrated on the 20-bit tag proposed by [13].

The layout of the original 20-bit chipless tag is composed of an array of U-shaped strip scatterers representing a bit word '11111111111111111111' (shown in Fig. 11a). The outer size of the largest element is 25.5 × 2.5 mm, while the dimensions of the smallest one equal 16 × 2.5 mm, with the strip width of 1 mm and the gap width equal to 0.5 mm. Consequently, all RCS resonance peaks match the frequency range from 2 to 4 GHz so that the performance of the tag would be comparable with those presented by Vena [13]. The distance between each two neighboring elements, which are arranged according to the element length from the longest one to the shortest one in descending order, is 1 mm. The tag motif was etched on the low-loss dielectric substrate Rogers RO4003 ($\varepsilon_r = 3.38$, tan $\delta = 0.002$) with the thickness of 0.2 mm. The incident excitation field is oriented parallel to the shortening strip stub placed at one end of each scatterer, i.e. horizontally to the tag presented in Fig. 11.

3.1 Scatterer Topology Modification

The proposed topology modification of the resonant folded dipoles consists in narrowing the strip width from original 1 mm to 0.25 mm to enable to taper the gap between the longitudinal dipole arms toward the open end to 0.5 mm. This taper shape reduces the mutual coupling between two neighboring coding particles, because their arms are more spatially separated.

Figure 7(a) shows the original U-folded dipole (UD) scatterer of the outer size of 20 × 2.5 mm with the 1 mm strip width and the gap of 0.5 mm in width, which is in accordance with [13]. The novel tapered U-folded dipole (T-UD) scatterer of the same outer size is depicted in Fig. 7(b).

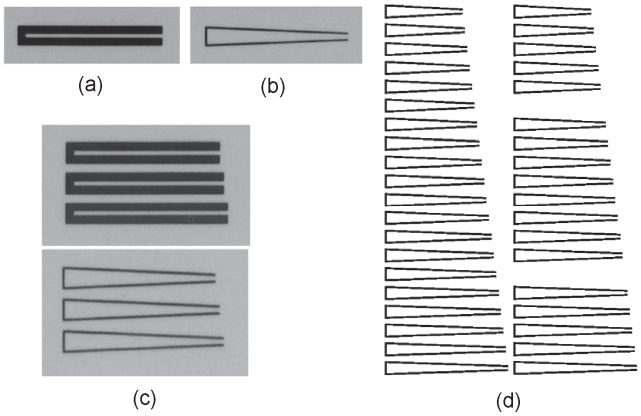

Fig. 7. Photograph of investigated modifications of folded-dipole scatterers: a) U-folded dipole (UD), b) tapered U-folded dipole (T-UD), c) their triplets, and d) 20-element arrays coding information 11111111111111111111 and 11111011111111011111 by leaving out the 6th and 15th elements.

To document the behavior of the proposed resonator topology, first resonator triplets were simulated by the CST Microwave Studio, fabricated and measured in the R32 waveguide. As it is indicated in Fig. 7(c), the fabricated triplets consist of three scatterers that are 20, 19.5, and 19 mm in length and of the same width. The distance among them at short ends is 1 mm, which is the same as in [13]. All scatterers are placed on the substrate that extends their dimensions by about 3 mm at each side of the scatterer.

As it can be seen in Fig. 8, the arrangement of particular scatterers closely spaced into the triplet detunes the resonant frequencies due to the mutual coupling. Namely in case of UD, we can apparently observe a noteworthy non-uniformity of RCS response magnitude. The tapering of gap between the dipole arms of the T-UD by about 4.5° from the original parallel direction reduces the mutual coupling. As a result, the amplitude uniformity of RCS response of T-UD is considerably improved.

To evaluate the performance of a larger structure, we simulated and measured 20-element arrays of both, the original UD and the proposed T-UD. Both of them were sequentially detuned by changing their lengths by 0.5 mm from 16 to 25.5 mm so that the outer sizes of the arrays were 69 × 25.5 mm^2. The evaluation of RCS of the fabricated tags was performed by one-port vector measurement of monostatic RCS in a free space, see Sec. 5. The horn antenna and scatterer array lied at the distance of approx. 19 cm. The tag RCS was evaluated using the method similar to that described in [13]. The simulations were performed by Zeland IE3D software.

The frequency range between the lowest and the highest resonant peaks of UD and T-UD are approx. 1.5 and 1.2 GHz, respectively; see Fig. 9(b). This means that the proposed 20-element T-UD array provides approx. 1.25 times higher information capacity per unit of the frequency range.

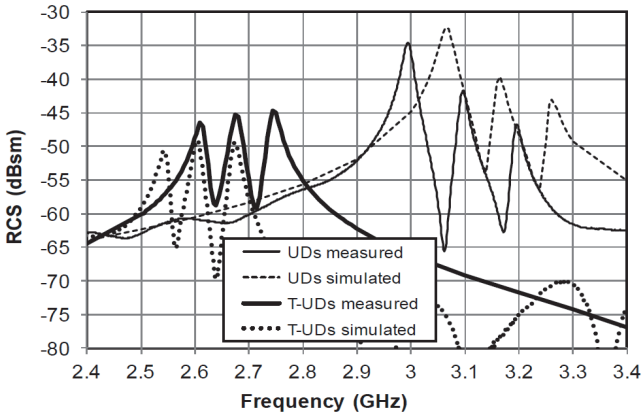

Fig. 8. Simulated and measured RCS response of triplets of original UD and T-UD.

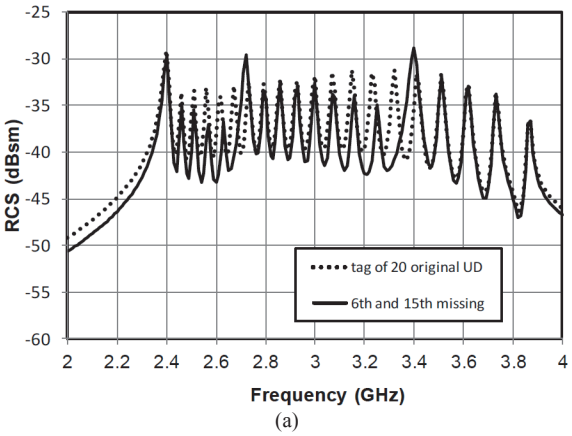

(a)

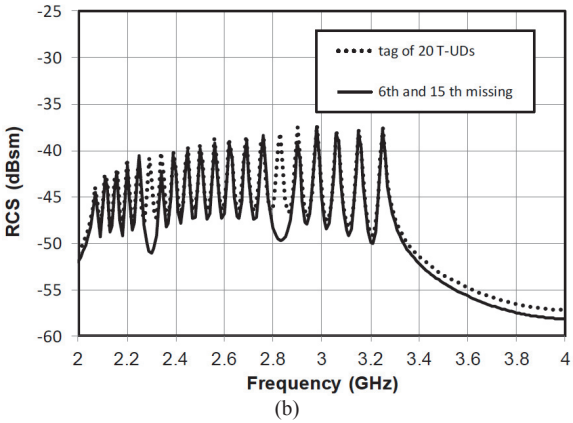

(b)

Fig. 9. Simulated RCS response of 20-element tags composed of original U-folded dipoles (a) and tapered U-folded dipoles (b) coding information 11111111111111111111 – tag with 20 elements, and 11111011111111011111 – tag coded by removed 6th and 15th elements.

In order to verify the influence of bit coding on the spectra shape, we removed the 6th and 15th scatterers, see Fig. 7(d) for the T-UD, and Fig. 12(a) for UD. We have found that the spectra of the original U-folded 20-element array exhibited an extensive change, namely in the case of resonant peaks neighboring the removed ones. These two peaks substantially alter their magnitudes; the lower one decreases, while the upper one increases by about 2 to

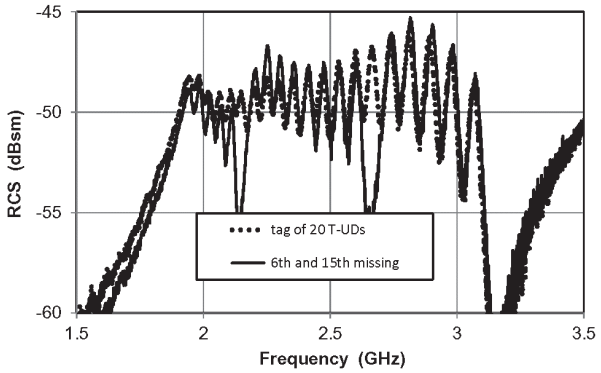

Fig. 10. Measured RCS response of 20-element tags composed of tapered U-folded dipoles coding information 11111111111111111111 – tag with 20 elements, and 11111011111111011111 – tag coded by removed the 6th and 15th elements.

3 dB. Furthermore, their resonant frequencies are detuned to the position of original resonance, see Fig. 9(a). The same effect is presented in the results of Vena et al., see Fig. 10 in [13].

Consequently, the "0" bits are nearly invisible in the tag spectral response. On the other hand, such unwanted behavior has not been observed in the case of 20-element T-UD array; see Fig. 9(b) showing the simulation results, and Fig. 10 indicating the measured data. The resonant peaks neighboring the missing peaks remain exactly in the same frequency position and their magnitude change is considerably smaller than in the case of UD array. Moreover, a better amplitude uniformity and frequency stability of the RCS response of T-UD compared to UD array is apparent.

In comparison to the UDs, the T-UDs have a smaller effective area due to tapering. It results in smaller RCS by approximately 7-10 dBsm, see Fig. 9. As a consequence, the sensitivity of the proposed tag is lower than the original one.

3.2 Scatterer Rearrangement in the Tag

To reduce the mutual coupling between the directly adjoining scatterers and the neighboring resonance frequencies so that the robustness of RCS curve is improved, we proposed a modification of element arrangement. The scatterers are divided into four sub-arrays, where each element is next to the one that was originally in fourth position from it. Consequently, the original ascending order according to the element length '1 2 3 4 5 6 7 ... 20' is modified to '1 5 9 13 17, 2 6 10 14 18, 3 7 11 15 19, 4 8 12 16 20'; see Fig. 11(b) and [24]. In this layout, the resonators with neighboring resonance frequencies are then located further apart and thus their coupling is substantially reduced. The third array configuration varies from the second configuration by the alignment of scatterers to the open end (see Fig. 11(c), which further increases the distance of shortening strip stubs of neighboring elements).

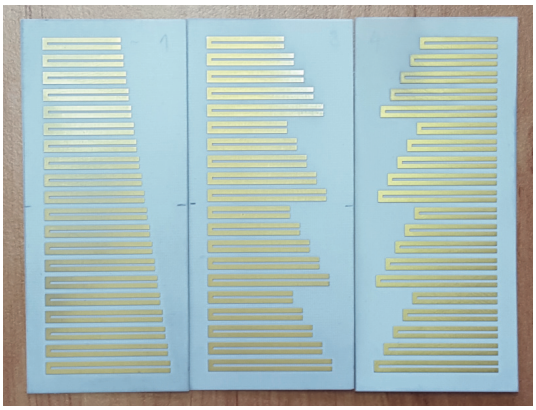

(a) (b) (c)

Fig. 11. Configurations of original and two modified layouts of 20-bit chipless tag, composed of array of U-shaped strip scatterers representing a bit word '11111111111111111111'. a) Original alignment to short ends, and element rearranged configurations with alignment b) novel alignment to short end, and c) to the open end.

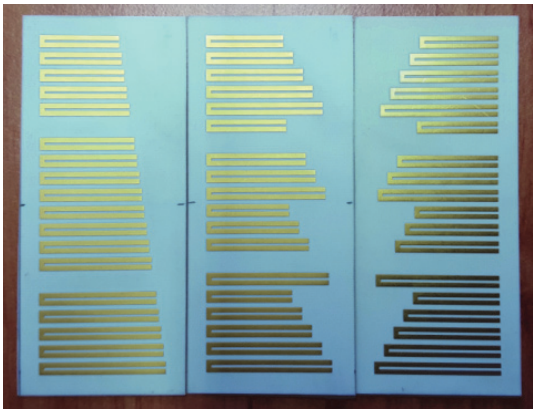

(a) (b) (c)

Fig. 12. Configurations of original and two modified layouts of 20-bit chipless tag, composed of array of U-shaped strip scatterers representing a bit word '11111011111111011111'. a) Original alignment to short ends, and element rearranged configurations with alignment b) novel alignment to short end, and c) novel alignment to the open end.

All three scatterer arrays (i.e. the reference and two arrays with element rearrangement) were tested for magnitude uniformity and frequency shift of RCS response using configuration of coding the '11111011111111011111' bit word. The polarization of incident electric field is oriented parallel to the short strip stub. The scatterers located in positions 6 and 15 (counted from the largest one) are missing; see Fig. 12.

The chipless tags were simulated by MoM software Zeland IE3D, using the infinite dielectric layer implementation with 20 cells per wavelength with narrow edge cells in order to perform a precise modeling of current density distribution in transversal cut of the strip. The RCS was calculated by IE3D from the field quantities for plane wave excitation.

The simulated RCS responses of 20-bit chipless tags, representing the bit words '11111111111111111111' (thin black line) and '11111011111111011111' (thick red line) are depicted in Fig. 13. In the case of reference tag (Fig. 13a), we can notice that due to removal of the 6th and 15th scatterers, the corresponding resonant peaks are missing. However, the magnitudes of lower neighboring resonant peaks considerably decreased, while the higher neighboring peaks registered the rise in their magnitudes. The overall magnitude uniformity is thus deteriorated. The difference between the highest (–30 dBsm) and the lowest (–40 dBsm) RCS magnitude peaks is about 10 dB. Moreover, we can see that the nearest lower and higher neighboring peaks slightly change their resonant frequencies in the direction to the original missing resonance. Thus, both the magnitude and frequency interval uniformity of RCS response are deteriorated. The dips in the characteristic corresponding to logical zeros are untraceable.

Furthermore, the lowest and the highest resonant peaks in RCS curve of bit word '11111111111111111111' are significantly higher and lower, respectively, than the

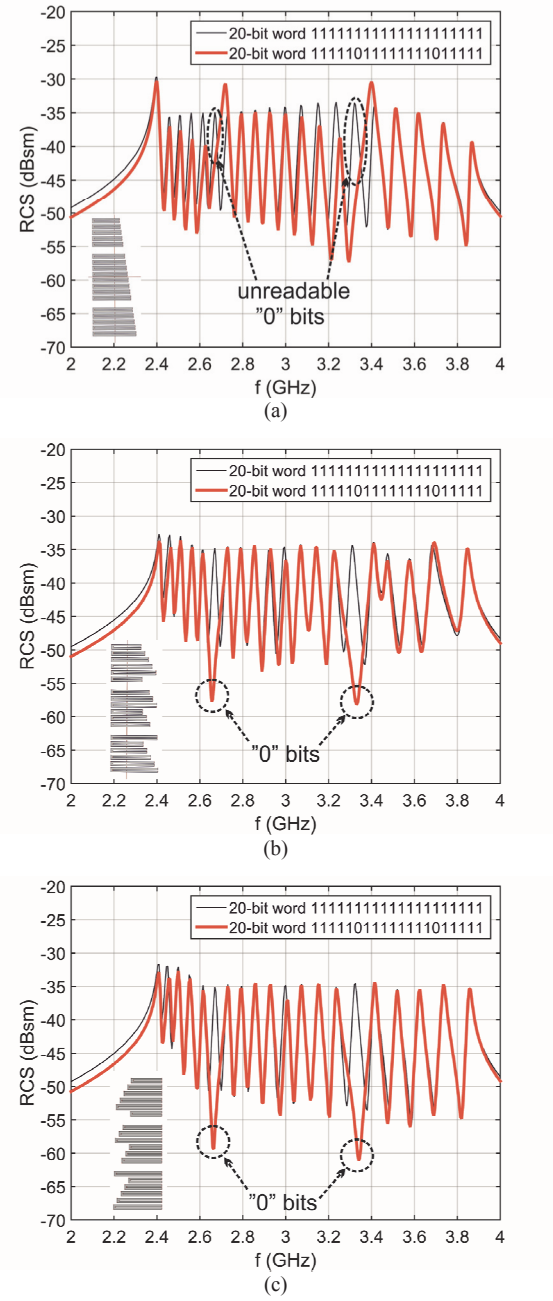

Fig. 13. Simulated RCS response of 20-bit chipless tag composed of array of U-shaped strip scatterers representing bit words '11111111111111111111' and '11111011111111011111' in (a) original alignment to short ends, and inter-element re-arrangement with alignment (b) to short ends, and (c) to open ends.

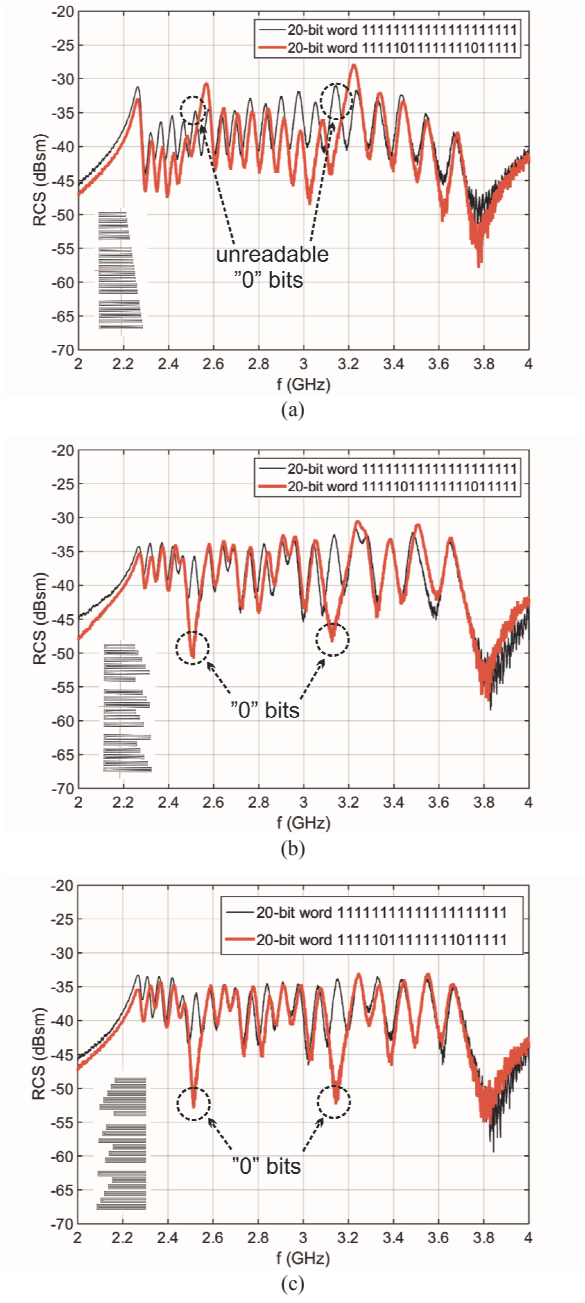

Fig. 14. Measured RCS response of 20-bit chipless tag composed of array of U-shaped strip scatterers representing bit words '11111111111111111111' and '11111011111111011111' in (a) original alignment to short ends, and inter-element re-arrangement with alignment (b) to short ends, and (c) to open ends.

rest of the inner peaks. On the other hand, both element-rearranged arrays coding the bit word ‘11111011111111011111’ exhibit missing resonances without the effect of distortion of magnitude and frequency interval uniformity of RCS curve; see Fig. 13(b), (c). The difference between the highest (–32 dBsm) and the lowest (–36 dBsm) RCS magnitudes is only about 4 dB.

The element-rearranged configuration with alignment to short ends exhibits a slightly higher magnitude distortion of the 16th to 18th resonant peaks. In addition, it is obvious that three lowest resonant peaks of the bit word ‘11111011111111011111’ are by about 2-3 dB higher than the rest of the peaks; see Fig. 13(b), (c). Figure 14 illustrates the measured RCS response of all three 20-bit chipless tags, original alignment to the short ends, inter-element rearrangement with alignment to the short ends, and to the open ends, representing the bit words ‘11111111111111111111’ and ‘11111011111111011111’.

The two element-rearranged tag configurations provide a comparable uniformity of the RCS curve. Nonetheless, the second configuration that is aligned to the scatterers’ open ends exhibits a slightly better amplitude and frequency stability of the RCS response.

4. Increasing of RCS Response Using Slot-in-Plate Scatterers

The read distance in specific chipless RFID applications may be limited due to the low RCS of their tags. We have therefore proposed a chipless RFID tag that offers a higher RCS at the level of –16 dBsm. This substantially enlarges the read distance compared to the value of RCS = –32 dBsm in Sec. 3.2. The tag is based on a complementary structure; coplanar slots are introduced in a metallic pattern, unlike the strip-based scatterers presented e.g. in [13], [14]. The basic pattern is a uniplanar rectangle etched on a thin dielectric substrate that displays a substantially higher RCS due to its large size relative to the wavelength that is used. An array of coplanar slots shorted at the one end is introduced into the surface of the rectangle. This pattern then exhibits a generally larger and typically monotone RCS curve over the selected frequency interval, with dips corresponding to the resonances of individual slots.

The tag is based on a metallic rectangular plate 52×50 mm^2 in size chosen to provide a monotonous RCS curve over the frequency range of 2 to 4 GHz [25]. Twenty shorted coplanar slots forming an inverted letter “U” are introduced symmetrically into the rectangle so that the slots are collinear with the unit polarization vector of the incident field. The vertical polarization of incident wave excites the electric field in the narrow shorted part of the slot; see Fig. 15.

The slot-arm length l ranges from 15.0 to 24.5 mm, with 0.5 mm in length difference between the two neighboring slot couple. The slot width is $w = 0.25$ mm and the

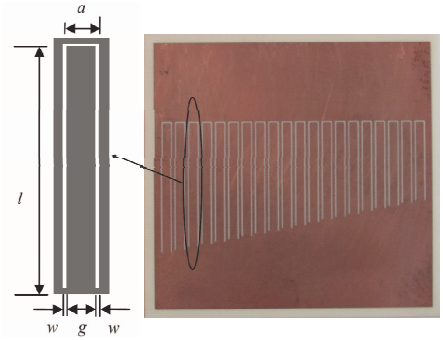

Fig. 15. Single coplanar slot width is etched in layout of the proposed 20-bit chipless RFID tag consisting of metallic rectangular plate with 18 shorted coplanar slots representing bit word ‘11111111111111111111’.

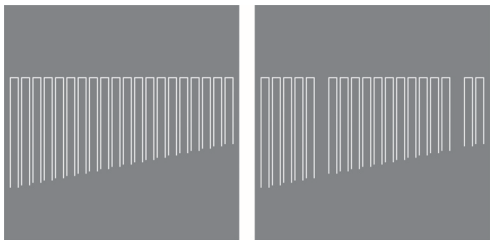

Fig. 16. Original arrangement of slots in rectangle representing 20-bit words ‘11111111111111111111’ (a) and ‘11111011111111111011’ (b).

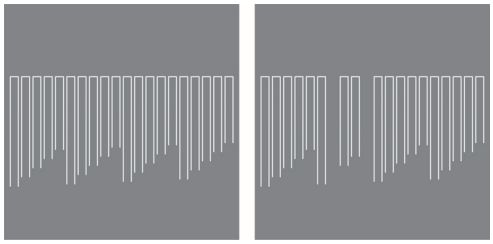

Fig. 17. Modified arrangement of slots in rectangle in the descending order according to their length, representing 20-bit words ‘11111111111111111111’ (a) and ‘11111011111111111011’ (b).

width of the shorting slot is $a = 2$ mm, so that the metallic gap between the two adjacent slot-arms equals $g = 1.5$ mm. The coplanar slots in an array are equidistant from each other, at a distance equal to 0.5 mm. The binary information is encoded into the slot array by presence of the slot symbolizing a notch in the RCS curve, and by absence of the slot representing a smooth RCS curve, see Figs. 16 and 17. A 20-element coplanar slot array with the 9th and 17th slots missing thus presents the 20-bit word ‘11111011111111111011’; see Fig. 17.

To verify the simulated results, see Figs. 18 and 19, we performed the monostatic measurement of tag RCS performance in the anechoic chamber; see Sec. 5. Figure 20 illustrates the measured RCS response of two variants of scatteres arrangement in 20-bit chipless RFID tags, i.e. with sequent arrangement and with re-arrangement of inter-elements representing comparison of bit words ‘11111111111111111111’ and ‘11111011111111111011’ for encoding by resonator removal.

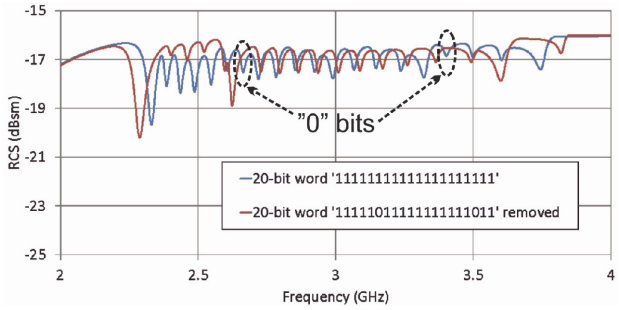

Fig. 18. Simulated RCS response of 20-element coplanar slot array with sequent arrangement of inter-elements representing comparison of bit words '11111111111111111111' and '11111011111111111011' for encoding by means of resonator removal.

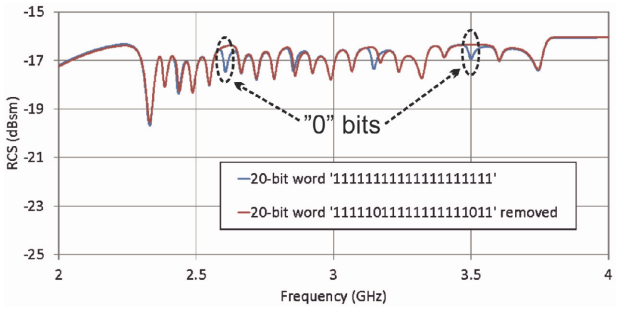

Fig. 19. Simulated RCS response of 20-element coplanar slot array with re-arrangement of inter-elements representing comparison of bit words '11111111111111111111' and '11111011111111111011' for encoding by resonator removal.

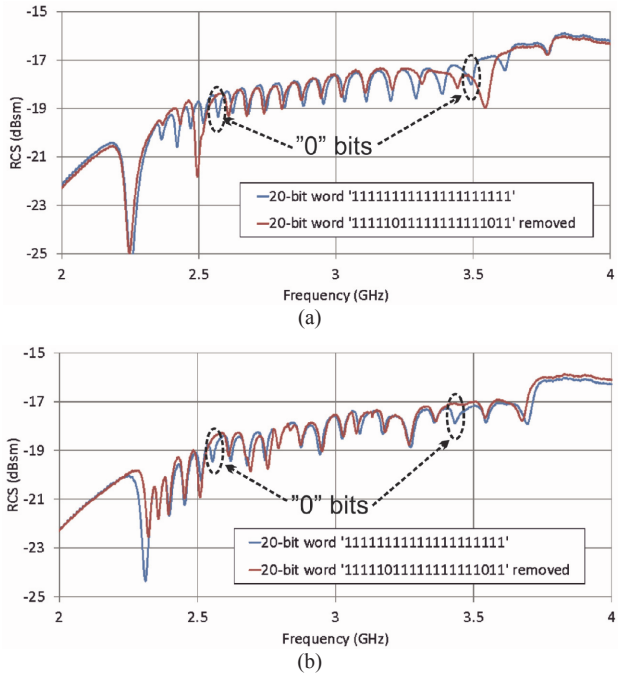

Fig. 20. Measured RCS response of 20-element coplanar slot array with sequent arrangement (a) and with re-arrangement of inter-elements (b) representing comparison of bit words '11111111111111111111' and '11111011111111111011' for encoding by resonator removal.

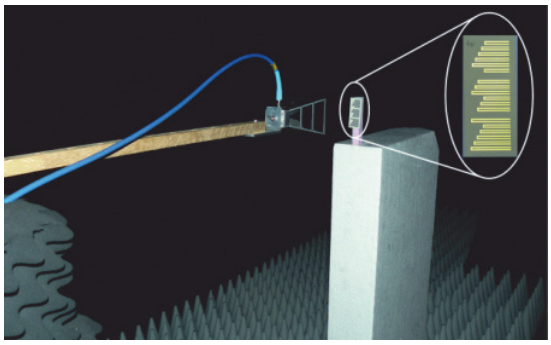

Fig. 21. Measurement setup using monostatic measurement configuration with detail of element-rearranged 20-bit tag.

5. Measurement Method

All aforementioned measured characteristics were obtained by monostatic measurement of tag RCS performance in the anechoic chamber; see Fig. 21. The measurement was based on the evaluation of reflection coefficient of the double ridge horn antenna DRH 20 [26] in front of which the scatterer at the distance of 0.3 m was placed. The calculation of RCS response of the tag was performed by the equation used in [13] and modified so that it was applicable to the case of the one-port measurement.

$$\sigma^{\text{tag}} = \left(\frac{S_{11}^{\text{tag}} - S_{11}^{\text{iso}}}{S_{11}^{\text{ref}} - S_{11}^{\text{iso}}} \right)^2 \sigma^{\text{ref}} \tag{1}$$

where S_{11}^{tag} is the reflection coefficient of the measured tag. S_{11}^{ref} represents the reflection coefficient of the reference plate used as a scatterer. S_{11}^{iso} symbolizes the reflection coefficient of the antenna itself in case that no scatterer is used, and comprises the residual reflection from the experimental surroundings. σ^{tag} stands for the RCS of the measured tag, σ^{ref} embodies the RCS of the reference scatterer, which is the rectangular ($a \times b$) metal plate 0.100×0.100 m^2 in size and 0.3 mm in thickness. Its analytical formula for RCS can be expressed as follows:

$$\sigma^{\text{ref}} = 4\pi \frac{a^2 b^2}{\lambda^2}. \tag{2}$$

6. Summary

The performance comparison of various types of planar scatterers for chipless RFID building elements shows that there is an expected trade-off between the electrical size and bandwidth on one side and the RCS level, representing reflection properties, on the other. Furthermore, it was found that the recently proposed arm loaded dipoles exhibit by up to 5–10 dB larger RCS level than U-folded dipoles of the same electrical size. Yet they provide typically a 2-3× larger bandwidth. It implies a smaller bit density in the unit frequency range. However, the best performance of the proposed loaded dipole S3 arm v2

($RCS = -33.5$ dBsm, $BW = 17.2$ dB, $ka = 0.35$) overcomes the reference U-folded dipole ($RSC = -5.0$ dBsm, $BW = 18.2$ dB, $ka = 0.62$) of the same outer dimensions.

Apart from the proper selection of scatterer topology for the highest BW-RCS product, the mutual coupling constitutes another important issue. Major distortion of RCS response is present when "0" bits are coded by removing appropriate scatterers. This is due to the electromagnetic interaction between the adjacent resonant elements placed in the array in the descending order in line with the resonant frequency. In such cases, the directly neighboring resonances are detuned from their original positions and RCS magnitudes are significantly changed. The proposed rearrangement of elements in the array is done in a way that the directly adjacent resonant elements are located further apart, which considerably improves the robustness and readability of RCS response.

The overall RCS response might be significantly improved provided that the interrogating signal is reflected from a larger radar target that contains band-notched resonators, such as slot-type elements placed in the planar rectangular element. There is an unresolved issue of proper topology of these band-notched resonators, which increases their quality factor so that the band dips reach the sufficient level.

The range of open challenges in the field of frequency-domain chipless RFID transponders involves further investigation into the optimal selection of scatterer element topology, the optimization of its geometrical parameters (aimed at maximization of the *RCS-BW-ka* product) and also the evaluation of influence of mutual coupling in the scatterer arrays on the overall RCS performance. The latter involves its robustness, reliable readability and achievable bit density in unit frequency range as well as in unit area.

Acknowledgments

This work was supported by the Czech Science Foundation under the project GA15-08803S "Remote Sensing of Small Scatterers by Electromagnetic Waves".

References

[1] DEY, S., SAHA, J., KARMAKAR, N. Smart sensing: Chipless RFID solutions for the Internet of everything. *IEEE Microwave Magazine*, 2015, vol. 16, no. 10, p. 26–39. DOI: 10.1109/MMM.2015.2465711

[2] HARROP, P., DAS, R. *Printed and Chipless RFID Forecasts, Technologies & Players 2011-2021.* [Online] Cited 2016-04-25. Available at: http://www.idtechex.com/research/reports/printed-and-chipless-rfid-forecasts-technologies-and-players-2011-2021-000254.asp.

[3] PRERADOVIC, S., KARMAKAR, N. *Fully Printable Chipless RFID Tag.* In *Advanced Radio Frequency Identification Design and Applications*. Ed. S. Preradovic. InTech, 2011. ISBN: 978-953-307-168-8

[4] PRERADOVIC, S., KARMAKAR, N. Chipless RFID: Bar code of the future. *IEEE Microwave Magazine*, 2010, vol. 11, no. 7, p. 87 to 97. DOI: 10.1109/MMM.2010.938571

[5] HARMA, S., PLESSKY, V. P. *Surface Acoustic Wave RFID Tags*. In *Development and Implementation of RFID Technology*. Ed. C. Turcu. InTech, 2009. ISBN: 978-3-902613-54-7

[6] NATIONAL INSTITUTE OF ADVANCED INDUSTRIAL SCIENCE AND TECHNOLOGY, JAPAN. *Printing of Organic Thin-Film Transistor Arrays on Flexible Substrates*. [Online] Cited 2016-04-25. Available at: http://www.aist.go.jp/aist_e/list/latest_research/2008/20080728/20080728.html

[7] GUPTA, S., NIKFAL, B., CALOZ, C. RFID system based on pulse-position modulation using group delay engineered microwave C-sections. In *2010 Asia-Pacific Microwave Conference*. Yokohama (Japan), 2010, p. 203-206. ISBN: 978-1-4244-7590-2

[8] HERRAIZ-MARTINEZ, F. J., PAREDES, F., GONZALEZ, G.Z., MARTIN, F., BONACHE, J. Printed magnetoinductive-wave (MIW) delay lines for chipless RFID applications. *IEEE Transactions on Antennas and Propagation*, 2012, vol. 60, no. 11, p. 5075–5082. DOI: 10.1109/TAP.2012.2207681

[9] VIOLINO, B. Firewall Protection for Paper Documents. *RFID Journal*. [Online] Cited 2016-04-25. Available at: http://www.rfidjournal.com/articles/view?790

[10] JONES, K. C. Invisible RFID Ink Safe for Cattle and People, Company Says. *Information Week.* [Online] Cited 2016-04-25. Available at: http://www.informationweek.com/invisible-rfid-ink-safe-for-cattle-and-people-company-says/d/d-id/1050602?

[11] MCVAY, J., HOORFAR, A., ENGHETA, N. Space-filling curve RFID tags. In *2006 IEEE Radio and Wireless Symposium*. San Diego (CA, USA), 2006, p. 199–202. DOI: 10.1109/RWS.2006.1615129

[12] PRERADOVIC, S., KARMAKAR, N. *Multiresonator-Based Chipless RFID*. Springer, 2012. ISBN: 978-1-4614-2094-1

[13] VENA, A., PERRET, E., TEDJINI, S. A fully printable chipless RFID tag with detuning correction technique. *IEEE Microwave and Wireless Components Letters*, 2012, vol. 22, no. 4. DOI: 10.1109/LMWC.2012.2188785

[14] VENA, A., PERRET, E., TEDJINI, S. A depolarizing chipless RFID tag for robust detection and its FCC compliant UWB reading system. *IEEE Transactions on Microwave Theory and Techniques,* 2013, vol. 61, no. 8, p. 2982–2994. DOI: 10.1109/TMTT.2013.2267748

[15] COSTA, F., GENOVESI, S., MONORCHIO, A. Chipless RFIDs for metallic objects by using cross polarization encoding. *IEEE Transactions on Antennas and Propagation,* 2014, vol. 62, no. 8, p. 4402–4407. DOI: 10.1109/TAP.2014.2326421

[16] REZAIESARLAK, R., MANTEGHI, M. Design of chipless RFID tags based on Characteristic Mode Theory (CMT). *IEEE Transactions on Antennas and Propagation,* 2015, vol. 63, no. 2, p. 711–718. DOI: 10.1109/TAP.2014.2382640

[17] SOMARK INNOVATIONS, INC. *About Us.* [Online] Cited 2016-04-25. Available at: http://www.somarkinnovations.com/about/

[18] GUILLET, A., VENA, A., PERRET, E., TEDJINI, S. Design of a chipless RFID sensor for water level detection. In *15th International Symposium on Antenna Technology and Applied Electromagnetics (ANTEM 2012)*. Toulouse (France), 2012, 4 p. DOI: 10.1109/ANTEM.2012.6262372

[19] AMIN, E. M., KARMAKAR, N. Partial discharge monitoring of High Voltage equipment using chipless RFID sensor. In *Asia-Pacific Microwave Conference 2011*. Melbourne (VIC, Australia), 2011, p. 1522–1525. ISBN: 978-1-4577-2034-5

[20] FENG, Y., XIE, L., CHEN, Q., ZHENG, L. R. Low-cost printed chipless RFID humidity sensor tag for intelligent packaging. *IEEE Sensors Journal*, 2015, vol. 15, no. 6, p. 3201–3208. DOI: 10.1109/JSEN.2014.2385154

[21] POLIVKA, M., MACHAC, J. Improvement of backscatter properties of C-shaped dipole scatterer for chipless RFID. In *Proceedings of Asia-Pacifc Microwave Conference.* Sendai (Japan), 2014, p. 962–964.

[22] POLIVKA, M., MACHAC, J. Novel size-reduced unit cells for uniplanar chipless RFID tags. In *Proceedings of Asia-Pacific Microwave Conference*. Seoul (Korea), 2013, p. 908–910. DOI: 10.1109/APMC.2013.6694970

[23] BEST, S. R., MORROW, J. D. On the significance of current vector alignment in establishing the resonant frequency of small space-filling wire antennas. *IEEE Antennas and Wireless Propagation Letters*, 2003, vol. 2, no. 1, p. 201–204. DOI: 10.1109/LAWP.2003.819686

[24] POLIVKA, M., HAVLICEK, J., SVANDA, M., MACHAC, J. Improvement of RCS response of U-shaped strip-based chipless RFID tags. In *Proceedings of European Microwave Conference (EuMC 2015)*. Paris (France), 2015, p. 107–110. DOI: 10.1109/EuMC.2015.7345711

[25] POLIVKA, M., SVANDA, M., MACHAC, J. Chipless RFID tag with an improved RCS response. In *Proceedings of the 44th European Microwave Conference (EuMC 2014).* Rome (Italy), 2014, p. 770–773. DOI: 10.1109/EuMC.2014.6986548

[26] RF SPIN S.R.O. *Model DRH20 - Double Ridge Waveguide Horn.* [Online] Cited 2016-04-25. Available at: http://www.rfspin.cz/en/antennas/drh20.php

About the Authors ...

Jaroslav HAVLICEK was born in Olomouc, Czechoslovakia, in 1989. He received his M.S. degree in Radio Electronics in 2015 from the Czech Technical University (CTU) in Prague, where he is currently doing a Ph.D. His thesis focuses on chipless RFID. He is the author or co-author of five papers published in international journals or conference proceedings.

Milan SVANDA was born in Prague, Czechoslovakia, in 1982. He received his M.S. and Ph.D. degrees in Radio Electronics in 2007 and 2011, respectively, both from the CTU in Prague, where he currently works as a research scientist. He is the author or co-author of more than 30 papers published in international journals or conference proceedings and co-author of five patents. His main research activities are focused on antennas operating in the close vicinity of human body, low-profile and wearable antennas and UHF RFID.

Jan MACHAC was born in Hranice, Czechoslovakia, in 1953. He graduated from the CTU in Prague in 1977. He received his CSc. (Ph.D. equivalent) in Electronics in 1982 at the Institution of Radio Engineering and Electronics of the Czechoslovak Academy of Science in Prague. He received his DrSc. degree in Radio Electronics in 1996 and was named a professor of Electrical Engineering in 2009. His main scientific interests cover investigation of planar passive elements and subsystems of microwave technology, propagation of electromagnetic waves in periodic structures and metamaterials. He is the author or co-author of more than 250 publications in scientific journals and scientific international as well as national conferences.

Milan POLIVKA was born in Prague, Czechoslovakia, in 1971. He received his M.S. and Ph.D. degrees in Radio Electronics in 1996 and 2003, respectively, both from the CTU in Prague, where he is currently holding the position of an associate professor. He is the author or co-author of more than 100 papers published in international journals or conference proceedings and co-author of seven patents. His research interests include antennas, artificial electromagnetic materials, RFID technology and applied electromagnetism.